MetaMorphs: Deformable Shape and Texture Models

Xiaolei Huang, Dimitris Metaxas, Ting Chen
Division of Computer and Information Sciences
Rutgers University – New Brunswick, NJ 08854, USA
{xiaolei, dnm}@cs.rutgers.edu, chenting@graphics.cis.upenn.edu

Abstract

We present a new class of deformable models, MetaMorphs, whose formulation integrates both shape and interior texture. The model deformations are derived from both boundary and region information based on a variational framework. This framework represents a generalization of previous parametric *and implicit* geometric *deformable models, by incorporating model interior texture information. The shape of the new model is represented implicitly as an "image" in the higher dimensional space of distance transforms. The interior texture is captured using a nonparametric kernel-based approximation of the intensity probability density function (p.d.f.) inside the model. The deformations that the model can undergo are defined using a space warping technique - the cubic B-spline based Free Form Deformations (FFD). When using the models for boundary finding in images, we derive the model dynamics from an energy functional consisting of both edge energy terms and texture energy terms. This way, the models deform under the influence of forces derived from both boundary and region information. A MetaMorph model can be initialized far-away from the object boundary and efficiently converge to an optimal solution. The proposed energy functional enables the model to pass small spurious edges and prevents it from leaking through large boundary gaps, hence makes the boundary finding robust to image noise and inhomogeneity. We demonstrate the power of our new models to segmentation applications, and various examples on finding object boundaries in noisy images with complex textures demonstrate the potential of the proposed technique.*

1. Introduction

Object boundary finding plays a fundamental role both in computer vision and in medical image analysis. It is also a challenging task due to the common presence of cluttered objects, complex backgrounds, noise and intensity inhomogeneity in natural and medical images. To address these difficulties, deformable model based segmentation approaches have been widely studied and used.

In *parametric* deformable models [5, 9, 10, 16], parametric curves/surfaces are used to represent the model's shape. Starting from an initial estimate, a deformable model evolves under the influence of both internal (e.g. smoothness) and external (e.g. image) forces to converge to the desired boundary of an image object. Traditionally, image forces come primarily from edge (image gradient) information. Such reliance on edge information, however, makes the models sensitive to noise and highly dependent on the initial estimate. In the past few years, there have been significant efforts to integrate region information into parametric deformable models. In [13], local region analysis strategies are introduced for Active Contour Models. However, the optimization of the integrated energy function is mostly heuristic. In [18], a generalized energy function that integrates region growing and boundary-based deformations is proposed. In this formulation, the parameters of the region intensity statistics can not be updated simultaneously with the boundary shape parameters so that the energy function has to be minimized in an iterative way. In hybrid segmentation frameworks proposed by [4, 8], a region based segmentation module is used to get a rough binary mask of the object of interest. Then this rough estimation of the object can be used to initialize a deformable model, which will deform to fit edge features in the image using the gradient information. In these frameworks, the region information and the boundary information are treated separately in different energy minimization processes so that the integration is still imperfect. As noted in [7], which uses active contours for region tracking applications, the difficulty in coupling region and boundary information is mostly due to the fact that the set of image regions does not have a structure of vector space, preventing us to use in a straightforward manner gradient descent methods, especially when statistical features of a region (such as mean and variance of intensity) are present. The authors turned to registration-like energy criterion to circumvent this problem.

Another line of research on deformable models are the

implicit geometric models [3, 11, 12, 14, 17], which are implemented in the level set based curve evolution framework. In the Mumford and Shah model for segmentation [11], an optimal piecewise smooth function is pursued to approximate an observed image, such that the function varies smoothly within each region, and rapidly or discontinuously across the boundaries of different regions. Solutions for the reduced cases of this minimal partition problem have been proposed in the level set framework [17]. In [12, 14], variational frameworks are proposed for image segmentation by unifying boundary and region-based information sources, and level set approaches are used to implement the resulting PDE systems. However, all these frameworks assume piecewise constant, or Gaussian intensity distributions within each partitioned region. This limits their power and robustness in finding objects whose interiors have high noise level, intensity inhomogeneity, and/or complex multi-modal intensity distributions. Furthermore, the computational cost of these level-set based implementations tends to be high.

To address the above limitations in previous efforts to incorporate region information in deformable models, we introduce in this paper a new class of deformable models, which we term "MetaMorphs". The MetaMorph models possess both shape and interior texture, and integrate boundary and region information coherently in a common variational framework. The model shapes in our framework are embedded in a higher dimensional space of distance transforms, thus represented by distance map "images". The model deformations are efficiently parameterized using the cubic B-spline based Free Form Deformations (FFD) [1, 2, 6]. The interior intensity statistics of the models are captured using nonparametric kernel-based approximations, which can represent complex multi-modal distributions. When finding object boundaries in images, the dynamics of the MetaMorph models are derived from an energy functional consisting of both edge/boundary energy terms and intensity/region energy terms. In our formulation, both types of energy terms are differentiable with respect to the model deformation parameters. This allows for a unified gradient-descent based deformation parameter updating paradigm using both boundary and region information. During model evolution, the boundary and region energy terms will have complementary effects. They will aid the model to grow/shrink and overcome local minima due to small spurious edges inside the object, to prevent the model from leaking at boundary gaps, and to enable the segmentation of objects with intensity inhomogeneity and complex interior statistics.

The remainder of the paper is organized as follows. In section 2, we introduce the shape and texture representations of the MetaMorph models. In section 3, we derive the MetaMorph model dynamics from both boundary and region information. In section 4, the overall model fitting algorithm and experimental results are presented, and we conclude with discussions in section 5.

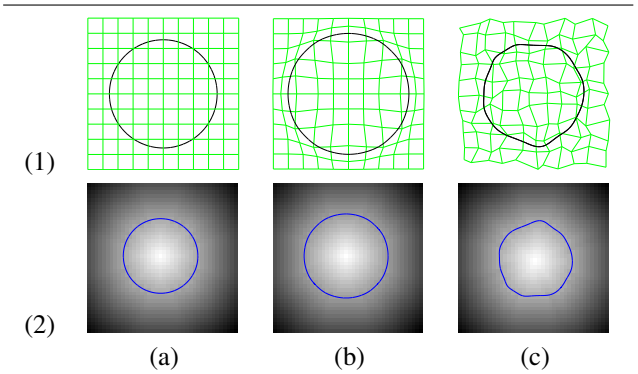

Figure 1. Shape representation and deformations of the MetaMorph models. (1) The model shape. (2) The implicit "image" representation of the model shape. (a) Initial model. (b) Example FFD control lattice deformation to expand the model. (c) Another example of the free-form model deformation given the control lattice deformation.

2. The MetaMorph Models

In this section, we present the shape and texture representations of the MetaMorph deformable models, and define the model deformations.

2.1. The Model's Shape Representation

The model's shape is embedded implicitly in a higher dimensional space of distance transforms. The Euclidean distance transform is used to embed an evolving model as the zero level set of a higher dimensional distance function. In order to facilitate notation, we consider the 2D case. Let $\Phi : \Omega \rightarrow R^+$ be a Lipschitz function that refers to the distance transform for the model shape $\mathcal{M}$. By definition Ω is bounded since it refers to the image domain. The shape defines a partition of the domain: the region that is enclosed by $\mathcal{M}$, $[\mathcal{R}_{\mathcal{M}}]$, the background $[\Omega - \mathcal{R}_{\mathcal{M}}]$, and on the model, $[\partial\mathcal{R}_{\mathcal{M}}]$ (In practice, we consider a narrow band around the model $\mathcal{M}$ in the image domain as $\partial\mathcal{R}_{\mathcal{M}}$). Given these definitions the following implicit shape representation is considered:

$$\Phi_{\mathcal{M}}(\mathbf{x}) = \begin{cases} 0, & \mathbf{x} \in \partial\mathcal{R}_{\mathcal{M}} \\ +ED(\mathbf{x}, \mathcal{M}) > 0, & \mathbf{x} \in \mathcal{R}_{\mathcal{M}} \\ -ED(\mathbf{x}, \mathcal{M}) < 0, & \mathbf{x} \in [\Omega - \mathcal{R}_{\mathcal{M}}] \end{cases}$$

where $ED(\mathbf{x}, \mathcal{M})$ refers to the min Euclidean distance between the image pixel location $\mathbf{x} = (x, y)$ and the model $\mathcal{M}$.

Such treatment makes the model shape representation an "image", which greatly facilitates the integration of boundary and region information. It also provides a feature space

in which objective functions that are optimized using a gradient descent method can be conveniently used. A sufficient condition for convergence of the gradient descent methods requires continuous first derivatives. The considered implicit representation satisfies such a condition. One can prove that the gradient of the distance function is a unit vector in the normal direction of the shape. This property will make our model evolution fast. Examples of this implicit representation can be found in [Fig. (1).2]. This shape representation in 3D is similarly defined in a volumetric embedding space.

2.2. The Model's Deformations

The deformations that MetaMorph models can undergo are defined using a space warping technique, the Free Form Deformations (FFD) [15]. The essence of FFD is to deform an object by manipulating a regular control lattice F overlaid on its volumetric embedding space. One of the main advantages of the FFD technique is that it imposes implicit smoothness constraints during deformation, since it guarantees C^1 continuity at control points and C^2 continuity everywhere else. Therefore there is no need for introducing computationally expensive regularization components on the deformed shapes. Another advantage is that, since FFD is a space warping technique, it integrates naturally with the implicit model shape representation in a higher dimensional embedding space. In this paper, we consider an Incremental Free Form Deformations (IFFD) formulation using the cubic B-spline basis [6].

Let us consider a regular lattice of control points

$$F_{m,n} = (F^x_{m,n}, F^y_{m,n});\ m = 1, ..., M, \quad n = 1, ..., N$$

overlaid to a region $\Gamma_c = \{\mathbf{x}\} = \{(x, y) | 1 \leq x \leq X, 1 \leq y \leq Y\}$ in the embedding space that encloses the model in its object-centered coordinate system. Let us denote the initial configuration of the control lattice as F^0, and the deforming control lattice as $F = F^0 + \delta F$. Under these assumptions, the incremental FFD parameters, which are also the deformation parameters for the model, are the deformations of the control points in both directions (x, y):

$$\mathbf{q} = \{(\delta F^x_{m,n}, \delta F^y_{m,n})\};\ (m, n) \in [1, M] \times [1, N]$$

The deformed position of a pixel $\mathbf{x} = (x, y)$ given the deformation of the control lattice from F^0 to F, is defined in terms of a tensor product of Cubic B-spline polynomials:

$$D(\mathbf{q}; \mathbf{x}) = \mathbf{x} + \delta D(\mathbf{q}; \mathbf{x}) = \sum_{k=0}^{3} \sum_{l=0}^{3} B_k(u) B_l(v) \\ (F^0_{i+k,j+l} + \delta F_{i+k,j+l}) \qquad (1)$$

where $i = \lfloor \frac{x}{X} \cdot (M-1) \rfloor + 1,\ j = \lfloor \frac{y}{Y} \cdot (N-1) \rfloor + 1$. The terms of the deformation component refer to:

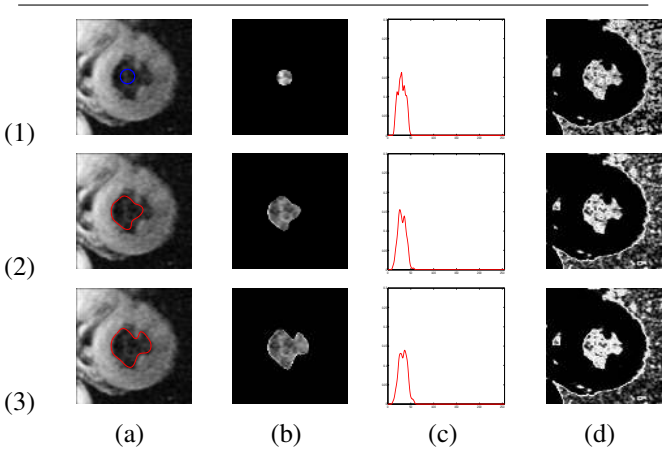

Figure 2. The Endocardium segmentation. (1) Initial model. (2) Intermediate result. (3) Final converged result. (a) The evolving model drawn in colored lines (blue or red) on original image. (b) Interior of the evolving model. (c) The intensity p.d.f of the model interior. The X axis is the intensity value in the range of $[0, 255]$ and the Y axis is the probability value in the range of $[0, 1]$. (d) The image probability map based on the p.d.f of the model interior.

- $\delta F_{i+l,j+l}$, $(k, l) \in [0, 3] \times [0, 3]$ are the deformations of pixel $\mathbf{x}$'s (sixteen) adjacent control points,
- $B_k(u)$ is the k^{th} basis function of a Cubic B-spine, defined by:

  $$B_0(u) = (1-u)^3/6,\ B_1(u) = (3u^3 - 6u^2 + 4)/6$$
  $$B_2(u) = (-3u^3 + 3u^2 + 3u + 1)/6,\ B_3(u) = u^3/6$$

  with $u = \frac{x}{X} \cdot (M-1) - \lfloor \frac{x}{X} \cdot (M-1) \rfloor$. $B_l(v)$ is similarly defined.
- $\delta D(\mathbf{q}; \mathbf{x}) = \sum_{k=0}^{3} \sum_{l=0}^{3} B_k(u) B_l(v) \delta F_{i+k,j+l}$ is the incremental deformation for pixel $\mathbf{x}$.

One example for the model deformations is shown in [Fig. (1)]. An initial model is shown in [Fig. (1).a], with regular control lattice. When its embedding space deforms due to the deformation of the FFD control lattice as shown in [Fig. (1).b], the model undergoes an expansion in its object-centered coordinate system. [Fig. (1).c] shows another example of free-form model deformation given the FFD control lattice deformation.

The extension of the models to account for deformations in 3D is straightforward, by using control lattices in the 3D space and a 3D tensor product of B-spline polynomials.

2.3. The Model's Texture

Rather than using traditional statistical parameters (such as mean and variance) to approximate the intensity distribution of the model interior, we model the distribution using

a nonparametric kernel-based method. The nonparametric approximation is differentiable, more generic and can represent complex multi-modal intensity distributions.

Suppose the model is placed on an image I, the image region bounded by current model $\Phi_{\mathcal{M}}$ is $\mathcal{R}_{\mathcal{M}}$, then the probability of a pixel's intensity value i being consistent with the model interior intensity can be derived using a Gaussian kernel as:

$$\mathbf{P}(i|\Phi_{\mathcal{M}}) = \frac{1}{V(\mathcal{R}_{\mathcal{M}})} \iint_{\mathcal{R}_{\mathcal{M}}} \frac{1}{\sqrt{2\pi}\sigma} e^{\frac{-(i-I(\mathbf{y}))^2}{2\sigma^2}} d\mathbf{y} \quad (2)$$

where $V(\mathcal{R}_{\mathcal{M}})$ denotes the volume of $\mathcal{R}_{\mathcal{M}}$, and σ is a constant specifying the width of the gaussian kernel.

Using this nonparametric approximation, the intensity distribution of the model interior gets updated automatically while the model deforms. The initialization of the model texture is flexible. We can either start with a small model inside the texture region to be segmented, or use supervised learning to specify the desired texture a Priori. One example of the model interior texture representation can be seen in [Fig. (2)]. In the figure, we show the zero level set of the current model $\Phi_{\mathcal{M}}$ in colored lines [Fig. (2).a], the model interior region $\mathcal{R}_{\mathcal{M}}$ [Fig. (2).b], the probability density function (p.d.f.) for the intensity of current model interior $\mathbf{P}(i|\Phi_{\mathcal{M}})$ for $i = 0, ...255$ [Fig. (2).c], and the probability map of every pixel's intensity in the image according to the model interior distribution [Fig. (2).d].

3. The MetaMorph Dynamics

We demonstrate the MetaMorph model fitting dynamics in the context object segmentation. However, the approach is general and can be applied to many other computer vision problems

In order to fit to the boundary of an object, the motion of the model is driven by both gradient (edge) energy terms and texture (intensity) energy terms derived from the image. The overall energy functional E consists of two parts – the shape data terms E_S, and the intensity data terms E_I:

$$E = E_S + kE_I \quad (3)$$

where k is a constant balancing the contribution of the two parts. In our formulation, we are able to omit the model smoothness term in traditional parametric or level-set based deformable models, since this smoothness is implicit by using the Free Form Deformations. Next, we derive the shape and intensity data terms respectively.

3.1. The Shape Data Terms

The gradient information is a very important source of the image forces for a deformable model. We encode the gradient information of an image using a "shape image" Φ, which is derived from the un-signed distance transform of the edge map of the image. In [Fig. (4).c], we can see the "shape image" of an example MR heart image.

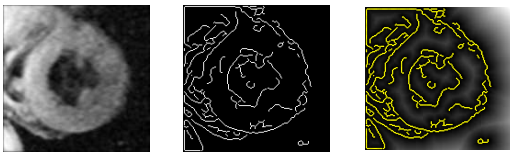

(a) (b) (c)

Figure 4. The effect of small spurious edges inside the object of interest (endocardium of the Left Ventricle) on the "shape image". (a) The original MR image. (b) The edge map of the image. (c) The derived "shape image", with edges points drawn in yellow. Note the effect of the small spurious edges on the "shape image" inside the object.

To evolve a MetaMorph model toward image edges, we define two shape data terms – an interior term E_{S_i} and a boundary term E_{S_b}:

$$E_S = E_{S_i} + aE_{S_b} \quad (4)$$

3.1.1. The Interior Shape Data Term In the interior shape data term of the model, we aim to minimize the Sum-of-Squared-Differences between the implicit shape representation values in the model interior and the underlying "shape image" values at corresponding deformed positions. This can be written as:

$$E_{S_i} = \frac{1}{V(\mathcal{R}_{\mathcal{M}})} \iint_{\mathcal{R}_{\mathcal{M}}} \left(\Phi_{\mathcal{M}}(\mathbf{x}) - \Phi(D(\mathbf{q};\mathbf{x}))\right)^2 d\mathbf{x} \quad (5)$$

During optimization, this term will deform the model along the gradient direction of the underlying "shape image". Thus it will expand or shrink the model accordingly, serving as a two-way balloon force without explicitly introducing such forces, and making the attraction range of the model large.

3.1.2. The Boundary Shape Data Term The previous interior shape term is good in attracting the model toward boundary structures from far-away locations. However, when there are small spurious edges detected within an object due to texture, the "shape image" inside the object could differ in the surrounding areas of those small edges. One such example can be seen in [Fig. (4).a-c]. To make the model deformation more robust to such situations, we consider a separated boundary shape data term, which allows higher weights for pixels in a narrow band around the model boundary $\partial\mathcal{R}_{\mathcal{M}}$.

$$E_{S_b} = \frac{1}{V(\partial\mathcal{R}_{\mathcal{M}})} \iint_{\partial\mathcal{R}_{\mathcal{M}}} \left(\Phi(D(\mathbf{q};\mathbf{x}))\right)^2 d\mathbf{x} \quad (6)$$

Intuitively, this term will encourage the deformation that maps the model boundary to the image edge locations where

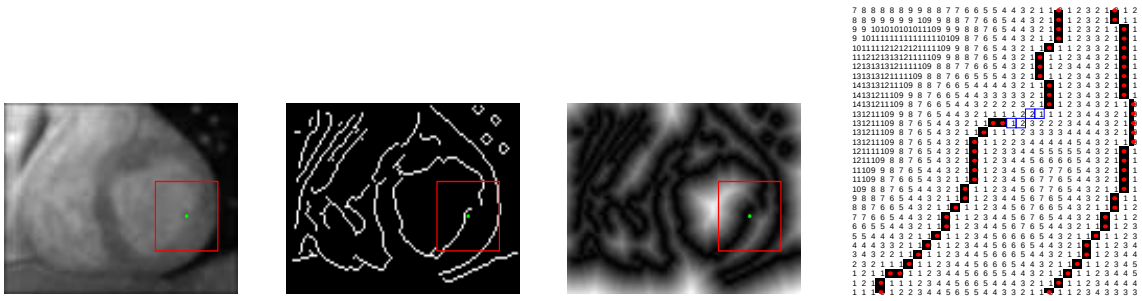

(a) (b) (c) (d)

Figure 3. The boundary shape data term constraints at small gaps in the edge map. (a) Original Image. (b) The edge map, note the small gap inside the red square region. (c) The "shape image". (d) Zoom-in view of the region inside the red square. The numbers are the "shape image" values at each pixel location. The red dots are edge points, the blue squares indicate a path favored by the boundary term for a MetaMorph model.

the underlying "shape image" distance values are as small (or as close to zero) as possible. In the shape energy functional [Eqn. (4)], by setting the value of constant $a > 1$, those model boundary pixels get higher weights.

One additional advantage of the boundary shape data term is that, at an edge with small gaps, this term will constrain the model to go along the "geodesic" path, which coincides with the smooth shortest path connecting the two open ends of a gap. This behavior can be seen from [Fig. (3)]. Note that at a small gap of the edge map, the boundary term will favor a path with the smallest accumulative distance values to the edge points.

3.2. The Intensity Data Terms

One of the most attractive aspects of our MetaMorph deformable models is that they possess interior texture, and their deformations are influenced by forces derived from image region information. This information is very important to help the models out of local minima, and converge to the true object boundaries. In [Fig. (4)], the spurious edges both inside and around the object boundary degrade the reliability of the "shape image" and the shape data terms. Yet the intensity probability map computed based on the interior texture of an initial model, as shown in [Fig. (2).1.d], gives a pretty clear indication of the rough boundary of the object. In another MR heart image shown in [Fig. (6).1.a], a large portion of the object (Endocardium) boundary is missing during computation of the edge map, due to errors in edge detection [Fig. (6).1.b]. Relying solely on the "shape image" [Fig. (6).1.c] and shape data terms, a model would have leaked through the large gap and mistakenly converged to the outer epicardium boundary. In this situation, the intensity probability maps [Fig. (6).2-4.d] computed based on the model interior statistics become the key to optimal model convergence.

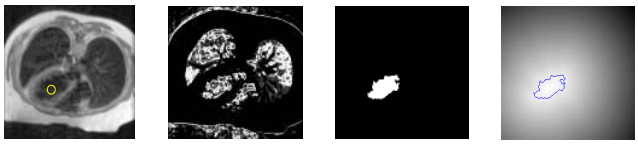

(a) (b) (c) (d)

Figure 5. Deriving the "region of interest" intensity data term. (a) The model shown (in yellow) on the original image. (b) The intensity probability map based on the model interior statistics. (c) The region of interest (ROI) derived from the thresholded probability map. The threshold is the mean probability over the entire image. (d) The "shape image" encoding boundary information of the ROI.

In our framework, the intensity energy function E_I consists of two intensity data terms – a "Region Of Interest" (ROI) term E_{I_r}, and a Maximum Likelihood term E_{I_m}:

$$E_I = E_{I_r} + bE_{I_m} \tag{7}$$

3.2.1. The ROI Intensity Data Term In the "Region Of Interest" (ROI) term, we aim to evolve the model toward the boundary of current region of interest, which is determined based on current model interior intensity distribution.

Given a model $\mathcal{M}$ on image I [Fig. (5).a], we first compute the image intensity probability map P_I [Fig. (5).b], based on the model interior intensity statistics (see section 2.3). Then a small threshold (typically the mean probability over the entire image domain) is applied on P_I to produce a binary image BP_I, in which pixels with probabilities higher than the threshold have value 1. Morphological operations are used to fill in small holes in BP_I. We then take the connected component on this binary image overlapping the model as current region of interest (ROI). Suppose the binary mask of this ROI is BI_r [Fig. (5).c], we en-

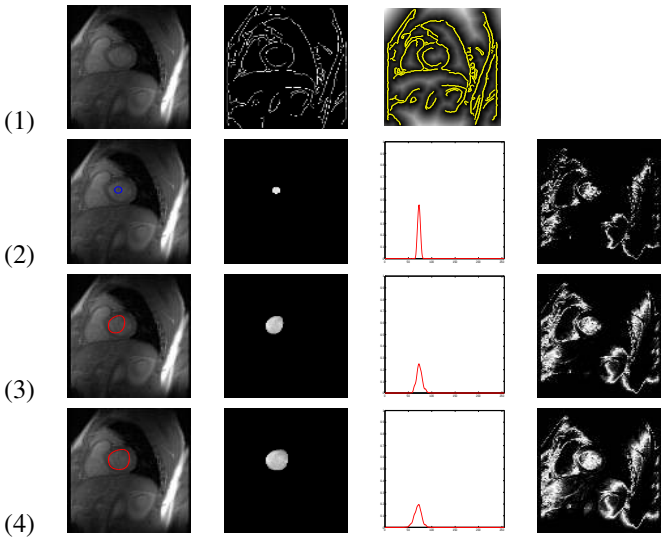

Figure 6. Segmentation of the Endocardium of the Left Ventricle in a MR image with a large portion of the object boundary edge missing. (1.a) The original image. (1.b) The edge map. (1.c) The "shape image". (2) Initial model, with zero level set model shape shown in blue. (3) Intermediate model, with zero level set model shape shown in red. (4) converged model. (a) current model on the image. (b) model interiors. (c) the interior intensity p.d.f.s. (d) intensity probability maps.

code its boundary information by computing the "shape image" of BI_r, which is the un-signed distance transform of the region boundary [Fig. (5).d]. Denote this "shape image" as Φ_r, the ROI intensity data term is defined as follows:

$$E_{I_r} = \frac{1}{V(\mathcal{R}_\mathcal{M})} \iint_{\mathcal{R}_\mathcal{M}} \big(\Phi_\mathcal{M}(\mathbf{x}) - \Phi_r(D(\mathbf{q};\mathbf{x}))\big)^2 d\mathbf{x} \quad (8)$$

This ROI intensity data term is the most effective in countering the effect of small spurious edges inside the object of interest (e.g. in Figs. (4,7). It also provides implicit balloon forces to quickly deform the model toward object boundary.

3.2.2. The Maximum Likelihood Intensity Data Term

The previous ROI intensity term is very efficient to deform the model toward object boundary when the model is still far-away. When the model gets close to the boundary, however, the ROI derived may become less reliable due to gradual intensity changes in the boundary areas. To achieve better convergence, we design another Maximum Likelihood (ML) intensity data term that constrains the model to deform toward areas where the pixel probabilities of belonging to the model interior intensity distribution are high. This ML term is formalized by maximizing the log-likelihood of pixel intensities in a narrow band around the model after deformation:

$$\begin{aligned} E_{I_m} &= -\tfrac{1}{V(\partial\mathcal{R}_\mathcal{M})} \iint_{\partial\mathcal{R}_\mathcal{M}} log\mathbf{P}(I(D(\mathbf{q};\mathbf{x}))|\Phi_\mathcal{M}) d\mathbf{x} \\ &= -\tfrac{1}{V(\partial\mathcal{R}_\mathcal{M})} \iint_{\partial\mathcal{R}_\mathcal{M}} \Big[log \tfrac{1}{V(\mathcal{R}_\mathcal{M})} + log \tfrac{1}{\sqrt{2\pi}\sigma} \\ &\quad + log \iint_{\mathcal{R}_\mathcal{M}} e^{\frac{-(I(D(\mathbf{q};\mathbf{x}))-I(\mathbf{y}))^2}{2\sigma^2}} d\mathbf{y} \Big] d\mathbf{x} \end{aligned} \quad (9)$$

During model evolution, when the model is still far away from object boundary, this ML term generates very little forces to influence the model deformation. When the model gets close to object boundary, however, the ML term generates significant forces to prevent the model from leaking through large gaps (e.g. in Fig. 6), and help the model to converge to the true object boundary.

3.3. Model Evolution

In our formulations above, both shape data terms and intensity data terms are differentiable with respect to the model deformation parameters $\mathbf{q}$, thus a unified gradient-descent based parameter updating scheme can be derived using both boundary and region information. Based on the definitions of the energy functions, one can derive the following evolution equation for each element $\mathbf{q}_i$ in the model deformation parameters $\mathbf{q}$:

$$\frac{\partial E}{\partial \mathbf{q}_i} = \big(\frac{\partial E_{S_i}}{\partial \mathbf{q}_i} + a\frac{\partial E_{S_b}}{\partial \mathbf{q}_i}\big) + k\big(\frac{\partial E_{I_r}}{\partial \mathbf{q}_i} + b\frac{\partial E_{I_m}}{\partial \mathbf{q}_i}\big) \quad (10)$$

- The motion due to the shape data terms are:

$$\begin{aligned} \frac{\partial E_{S_i}}{\partial \mathbf{q}_i} &= \frac{1}{V(\mathcal{R}_\mathcal{M})} \iint_{\mathcal{R}_\mathcal{M}} 2\big(\Phi_\mathcal{M}(\mathbf{x}) - \Phi(D(\mathbf{q};\mathbf{x}))\big) \cdot \\ &\quad \big(-\nabla\Phi(D(\mathbf{q};\mathbf{x})) \cdot \frac{\partial}{\partial \mathbf{q}_i} D(\mathbf{q};\mathbf{x})\big) d\mathbf{x} \end{aligned}$$

$$\begin{aligned} \frac{\partial E_{S_b}}{\partial \mathbf{q}_i} &= \frac{1}{V(\partial\mathcal{R}_\mathcal{M})} \iint_{\partial\mathcal{R}_\mathcal{M}} 2\Phi(D(\mathbf{q};\mathbf{x})) \cdot \\ &\quad \big(\nabla\Phi(D(\mathbf{q};\mathbf{x})) \cdot \frac{\partial}{\partial \mathbf{q}_i} D(\mathbf{q};\mathbf{x})\big) d\mathbf{x} \end{aligned}$$

- And the motion due to the intensity data terms are:

$$\begin{aligned} \frac{\partial E_{I_r}}{\partial \mathbf{q}_i} &= \frac{1}{V(\mathcal{R}_\mathcal{M})} \iint_{\mathcal{R}_\mathcal{M}} 2\big(\Phi_\mathcal{M}(\mathbf{x}) - \Phi_r(D(\mathbf{q};\mathbf{x}))\big) \cdot \\ &\quad \big(-\nabla\Phi_r(D(\mathbf{q};\mathbf{x})) \cdot \frac{\partial}{\partial \mathbf{q}_i} D(\mathbf{q};\mathbf{x})\big) d\mathbf{x} \end{aligned}$$

$$\begin{aligned} \frac{\partial E_{I_m}}{\partial \mathbf{q}_i} &= -\frac{1}{V(\partial\mathcal{R}_\mathcal{M})} \iint_{\partial\mathcal{R}_\mathcal{M}} \Big[\Big(\iint_{\mathcal{R}_\mathcal{M}} e^{\frac{-(I(D(\mathbf{q};\mathbf{x}))-I(\mathbf{y}))^2}{2\sigma^2}} d\mathbf{y} \Big)^{-1} \\ &\quad \iint_{\mathcal{R}_\mathcal{M}} e^{\frac{-(I(D(\mathbf{q};\mathbf{x}))-I(\mathbf{y}))^2}{2\sigma^2}} \cdot \Big(-\frac{(I(D(\mathbf{q};\mathbf{x})) - I(\mathbf{y}))}{\sigma^2} \cdot \\ &\quad \big(\nabla I(D(\mathbf{q};\mathbf{x})) \cdot \frac{\partial}{\partial \mathbf{q}_i} D(\mathbf{q};\mathbf{x})\big)\Big) d\mathbf{y} \Big] d\mathbf{x} \end{aligned}$$

In the above formulas, the partial derivatives with respect to the deformation (FFD) parameters, $\frac{\partial}{\partial \mathbf{q}_i} D(\mathbf{q};\mathbf{x})$, can be easily derived from the model deformation formula for $D(\mathbf{q};\mathbf{x})$ [Eqn. (1)]. Details are given in the Appendix.

4. The Model Fitting Algorithm and Experimental Results

The overall model fitting algorithm consists of the following steps:

1. Initialize the deformation parameters $\mathbf{q}$ to be $\mathbf{q}^0$, which indicates no deformation.
2. Compute $\frac{\partial E}{\partial \mathbf{q}_i}$ for each element $\mathbf{q}_i$ in the deformation parameters $\mathbf{q}$.
3. Update the parameters $\mathbf{q}_i' = \mathbf{q}_i - \lambda \cdot \frac{\partial E}{\partial \mathbf{q}_i}$.
4. Using the new parameters, compute the new model $\mathcal{M}' = D(\mathbf{q}'; \mathcal{M})$.
5. Update the model. Let $\mathcal{M} = \mathcal{M}'$, re-compute the implicit representation of the model $\Phi_{\mathcal{M}}$, and the new partitions of the image domain by the new model: $[\mathcal{R}_{\mathcal{M}}]$, $[\Omega - \mathcal{R}_{\mathcal{M}}]$, and $[\partial \mathcal{R}_{\mathcal{M}}]$. Also re-initialize a regular FFD control lattice to cover the new model, and update the "region of interest" shape image ϕ_r based on the new model interior.
6. Repeat steps 1-5 until convergence.

In the algorithm, after each iteration, both shape and interior intensity statistics of the model get updated based on the model dynamics, and deformation parameters get re-initialized for the new model. This allows continuous, both large-scale and small-scale deformations for the model to converge to the energy minimum.

In order to achieve good performance, the three weight factors, k, a and b in the energy functional (see [Eqn. (10)]) need to be assigned with care. In the current protocol we use, we always assign higher weights to data terms consisting of model boundary pixels, i.e. the boundary shape data term E_{S_b} and the Maximum Likelihood intensity data term E_{I_m}. Thus we set $a > 1, b > 1$. The weighting factor between the shape terms and intensity terms, k, is determined by a confidence measure, C_e, of the computed edge map. To decide this confidence value, we compute the "region of interest" (see section 3.2.1) after initializing a model, then C_e is determined by the complexity of the original image gradient or edge map in this ROI. The confidence value is low if there are high gradient and edges inside the region; the value is high, otherwise. Then we set the value for the weighting factor $k = \frac{1}{C_e}$.

Some examples of using our MetaMorph models and the weighting factors described above for boundary finding in images have been shown in [Fig. (2)] and [Fig. (6)]. In [Fig. (7)], we show another example in which we segment the Endocardium of the left ventricle in a noisy tagged MR heart image. Note that, due to the tagging lines and intensity inhomogeneity, the detected edges of the object are fragmented, and there are spurious small edges inside the region. In this case, the integration of both shape and texture information is critical in helping the model out of local minima.

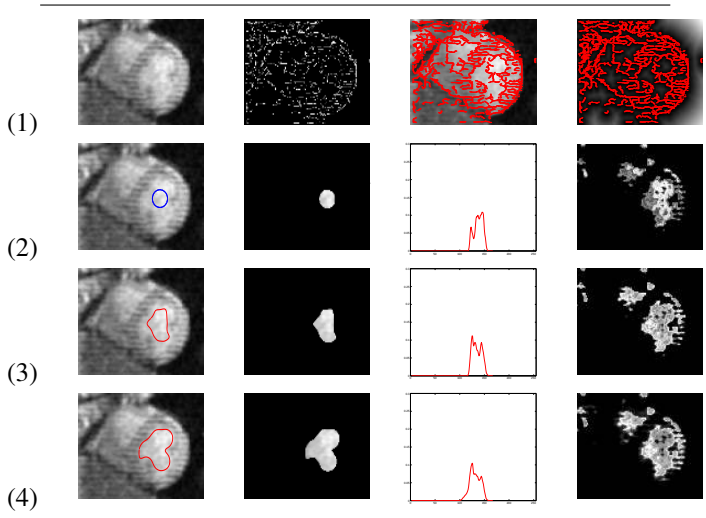

Figure 7. The tagged MR heart image. (1.a) The original image. (1.b) The edge map. (1.c) The edge points overlaid on original image. (1.d) The "shape image". (2) Initial model. (3) Intermediate result. (4) Final model (after 50 iterations). (2-4)(a) The evolving model. (2-4)(b) The model interior. (2-4)(c) The model interior intensity probability density. (2-4)(d) The intensity probability map of the image based on the p.d.f in (c).

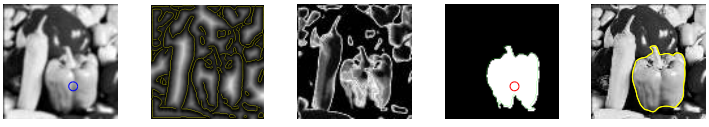

Figure 8. Boundary finding in the pepper image. (a) Original image, with initial model drawn in blue. (b) The shape image derived from edge map, with edges drawn in yellow. (c) The intensity probability map derived based on model interior statistics. (d) Region of Interest (ROI) extracted. (e) Final segmentation result.

On natural images, we show an example using the pepper image in [Fig. (8)]. Starting from a small model initialized inside the object, the model quickly deforms to the object boundary. In this example, a low weight is given to the interior shape data term due to the spurious edges inside the "region of interest". High weights are given to both boundary shape term and maximum likelihood intensity term so that the converged model is optimized on the boundary.

The MetaMorph model evolution is computationally efficient, due to our use of the FFD parameterization of the

model deformations. For all the examples shown, the segmentation process takes less than $200ms$ to converge on a 2Ghz PC station.

5. Conclusions

In this paper, we have presented a new class of deformable models, MetaMorphs, which possess both boundary shape and interior intensity statistics. In our framework, boundary and region information are coupled coherently to drive the deformations of the models toward object boundaries. This framework represents a generalization of previous *parametric* and *geometric* deformable models, to take into account model interior texture information. It does not require learning statistical shape and appearance models *a priori*, but the model deformations are constrained such that interior statistics of the models after deformation are consistent with the statistics learned from the past history of the model interiors. The algorithm can be straightforwardly applied in 3D, and can handle efficiently the merging of multiple models that are evolving simultaneously.

In our future work, we will conduct more principled and quantitative study in assigning the weight factors between the energy function components, and validate the segmentation results. We will also extend the framework to deal with large-scale textures, using gabor filters and other related techniques.

Appendix

We can analytically derive the partial derivatives $\frac{\partial}{\partial \mathbf{q}_i} D(\mathbf{q}; \mathbf{x})$ for the incremental B-spline FFD parameters in $\mathbf{q}$:

$$\delta F_{m,n} = (\delta F^x_{m,n}, \delta F^y_{m,n});\ m = 1, ..., M, \quad n = 1, ..., N$$

Without loss of generality, one can consider the $(m, n)th$ control point and its deformations in both directions. Then, from the definition for the deformations $D(\mathbf{q}; \mathbf{x})$, the following relations hold:

$$\frac{\partial\, \delta D(\mathbf{q}; \mathbf{x})}{\partial \delta F^x_{m,n}} = \begin{cases} \begin{bmatrix} B_{m-i}(u)\, B_{n-j}(v) \\ 0 \end{bmatrix}, 0 \le m - i, n - j \le 3 \\ \mathbf{0}, \qquad otherwise \end{cases}$$

$$\frac{\partial\, \delta D(\mathbf{q}; \mathbf{x})}{\partial \delta F^y_{m,n}} = \begin{cases} \begin{bmatrix} 0 \\ B_{m-i}(u)\, B_{n-j}(v) \end{bmatrix}, 0 \le m - i, n - j \le 3 \\ \mathbf{0}, \qquad otherwise \end{cases}$$

Acknowledgments

This research has been supported by the NSF-0205671 grant. We also would like to acknowledge many stimulating discussions with Nikos Paragios and Chenyang Xu.

References

[1] A. A. Amini, Y. Chen, M. Elayyadi, and P. Radeva. Tag surface reconstruction and tracking of myocardial beads from SPAMM-MRI with parametric b-spline surfaces. *IEEE Transactions on Medical Imaging*, 20(2):94–103, 2001.

[2] E. Bardinet, L. D. Cohen, and N. Ayache. A parametric deformable model to fit unstructured 3D data. *Computer Vision and Image Understanding*, 71(1):39–54, 1998.

[3] V. Caselles, R. Kimmel, and G. Sapiro. Geodesic active contours. In *IEEE Int'l Conf. on Computer Vision*, pages 694–699, 1995.

[4] T. Chen and D. Metaxas. Image segmentation based on the integration of markov random fields and deformable models. In *Proc. of Int'l Conf. on Medical Imaging Copmuting and Computer-Assisted Intervention*, pages 256–265, 2000.

[5] L. D. Cohen and I. Cohen. Finite-element methods for active contour models and balloons for 2-D and 3-D images. *IEEE Trans. on Pattern Analysis and Machine Intelligence*, 15:1131–1147, 1993.

[6] X. Huang, N. Paragios, and D. Metaxas. Establishing local correspondences towards compact representations of anatomical structures. In *Proc. of Int'l Conf. on Medical Imaging Computing and Computer-Assisted Intervention, LNCS 2879*, pages 926–934, 2003.

[7] S. Jehan-Besson, M. Barlaud, and G. Aubert. Shape gradients for histogram segmentation using active contours. In *IEEE Int'l Conf. on Computer Vision*, pages 408–415, 2003.

[8] T. Jones and D. Metaxas. Automated 3D segmentation using deformable models and fuzzy affinity. In *Proc. of Information Processing in Medical Imaging*, pages 113–126, 1997.

[9] M. Kass, A. Witkin, and D. Terzopoulos. Snakes: Active contour models. *Int'l Journal of Computer Vision*, 1:321–331, 1987.

[10] D. Metaxas. *Physics-Based Deformable Models*. Kluwer Academic Publishers, 1996.

[11] D. Mumford and J. Shah. Optimal approximations by piecewise smooth functions and associated variational problems. *Communications on Pure and Applied Mathematics*, 42(5):577–685, 1989.

[12] N. Paragios and R. Deriche. Geodesic active regions and level set methods for supervised texture segmentation. *Int'l Journal of Computer Vision*, 46(3):223–247, 2002.

[13] R. Ronfard. Region-based strategies for active contour models. *International Journal of Computer Vision*, 13(2):229–251, 1994.

[14] M. Rousson and R. Deriche. A variational framework for active and adaptive segmentation of vector valued images. In *Proceedings of the IEEE Workshop on Motion and Video Computing, Orlando, Florida*, Dec. 2002.

[15] T. W. Sederberg and S. R. Parry. Free-form deformation of solid geometric models. In *Proceedings of the 13th Annual Conference on Computer Graphics*, pages 151–160, 1986.

[16] L. H. Staib and J. S. Duncan. Boundary finding with parametrically deformable models. *IEEE Transactions on Pattern Analysis and Machine Intelligence*, 14(11):1061–1075, 1992.

[17] L. A. Vese and T. F. Chan. A multiphase level set framework for image segmentation using the Mumford and Shah model. *Int'l Journal of Computer Vision*, 50(3):271–293, 2002.

[18] S. Zhu and A. Yuille. Region Competition: Unifying snakes, region growing, and Bayes/MDL for multi-band image segmentation. *IEEE Trans. on Pattern Analysis and Machine Intelligence*, 18(9):884–900, 1996.